Journal of Molecular and Cellular Cardiology 114 (2018) 234–242

Contents lists available at ScienceDirect

Journal of Molecular and Cellular Cardiology

journal homepage: www.elsevier.com/locate/yjmcc

Original article

Characteristics of induced pluripotent stem cells from clinically divergent female monozygotic twins with Danon disease

Shohei Yoshida[a], Chiaki Nakanishi[a,*], Hirofumi Okada[a], Masayuki Mori[a], Junichiro Yokawa[a], Tsuyoshi Yoshimuta[a], Kunio Ohta[b], Tetsuo Konno[a], Noboru Fujino[a], Masa-aki Kawashiri[a], Akihiro Yachie[b], Masakazu Yamagishi[a], Kenshi Hayashi[a]

[a] Department of Cardiovascular and Internal Medicine, Kanazawa University Graduate School of Medicine, Kanazawa, Japan
[b] Department of Pediatrics, Kanazawa University Graduate School of Medicine, Kanazawa, Japan

ARTICLE INFO

Keywords:
Danon disease
LAMP2
iPS cells
X-chromosome inactivation
Identical twins

ABSTRACT

Rationale: Induced pluripotent stem cells (iPSCs) have been generated from patients with various forms of disease, including Danon disease (DD); however, few reports exist regarding disease-specific iPSCs derived from clinically divergent monozygotic twins.

Objective: We examined the characteristics of iPSCs and iPSC-derived cardiomyocytes (iPSC-CMs) generated from clinically divergent monozygotic female twins with DD.

Methods and results: We generated iPSCs derived from T-cells isolated from clinically divergent, 18-year-old female twins with DD harboring a mutation in *LAMP2* at the intron 6 splice site (IVS6 + 1_4delGTGA). Two divergent populations of iPSCs could prepare from each twin despite of their clinical divergence: one with wild-type LAMP2 expression (WT-iPSCs) and a second with mutant LAMP2 expression (MT-iPSCs). The iPSCs were differentiated into iPSC-CMs and then autophagy failure was observed only in MT-iPSC-CMs by electron microscopy, tandem fluorescent-tagged LC3 analysis, and LC3-II western blotting. Under these conditions, X-chromosome inactivation (XCI) was determined by PCR for the (CAG)n repeat in the androgen receptor gene, revealing an extremely skewed XCI pattern with the inactivated paternal wild-type and maternal mutant X-chromosomes in MT-iPSCs and WT-iPSCs, respectively, from each twin.

Conclusion: Regardless of their clinical differences, we successfully established two sets of iPSC lines that expressed either wild-type or mutant LAMP2 allele from each monozygotic twin with DD, of which only the populations expressing mutant LAMP2 showed autophagic failure.

1. Introduction

Danon disease (DD) is an X-linked disorder clinically characterized by hypertrophic cardiomyopathy, skeletal myopathy, and intellectual disability induced by mutations in *LAMP2*[1,2]. Female carriers are usually asymptomatic in childhood, although a fixed percentage of patients show symptoms in adulthood with varying degrees of severity [3]. We recently reported a rare case of monozygotic female twins with DD harboring a *LAMP2* splicing mutation (IVS6 + 1_4delGTGA) [4]. Interestingly, the patients showed divergent clinical appearance despite a similar environment [4].

Induced pluripotent stem cells (iPSCs) are generated by reprogramming somatic cells and capable of self-renewal and differentiation into all three germ layers [5,6]. Since then, various disease-specific iPSCs have been created [7–11], including those of X-linked disorders—such as Duchenne muscular dystrophy, hemophilia, and DD [12–14]. A few reports have used female carrier-derived iPSCs to model X-linked disease [15–18], since X-chromosome inactivation (XCI) is a unique feature of female iPSCs. Interestingly, the generated iPSCs showed different XCI patterns and phenotypes, and because of the hidden clinical phenotype, whether the generated iPSC line modeled the carrier or not is difficult to evaluate. Furthermore, whether the iPSCs from the patients with X-linked disease with clinical phenotype demonstrates equivalent phenotype to the iPSCs from the carrier with

Abbreviations: DD, Danon disease; LAMP2, lysosome associated membrane protein 2; XCI, X-chromosome inactivation; iPSCs, induced pluripotent stem cells; iPSC-CMs, induced pluripotent stem cells derived cardiomyocytes like cells; PBMCs, peripheral blood mononuclear cells; mAb, monoclonal antibody; MEFs, mouse embryonic fibroblasts; KSR, Knock-out Serum Replacement; bFGF, basic fibroblast growth factor; AVs, autophagic vacuoles; tfLC3, tandem fluorescent-tagged LC3; TEM, Transmission Electron Microscopy; H3K27me3, Trimethyl-Histone H3 (Lys27); AR, androgen receptor

* Corresponding author at: Department of Cardiovascular and Internal Medicine, Kanazawa University Graduate School of Medicine, Takara-machi 13-1, Kanazawa 920-8641, Japan.
E-mail address: n_chiaki0815@staff.kanazawa-u.ac.jp (C. Nakanishi).

https://doi.org/10.1016/j.yjmcc.2017.11.019
Received 19 July 2017; Received in revised form 4 November 2017; Accepted 22 November 2017
Available online 23 November 2017
0022-2828/

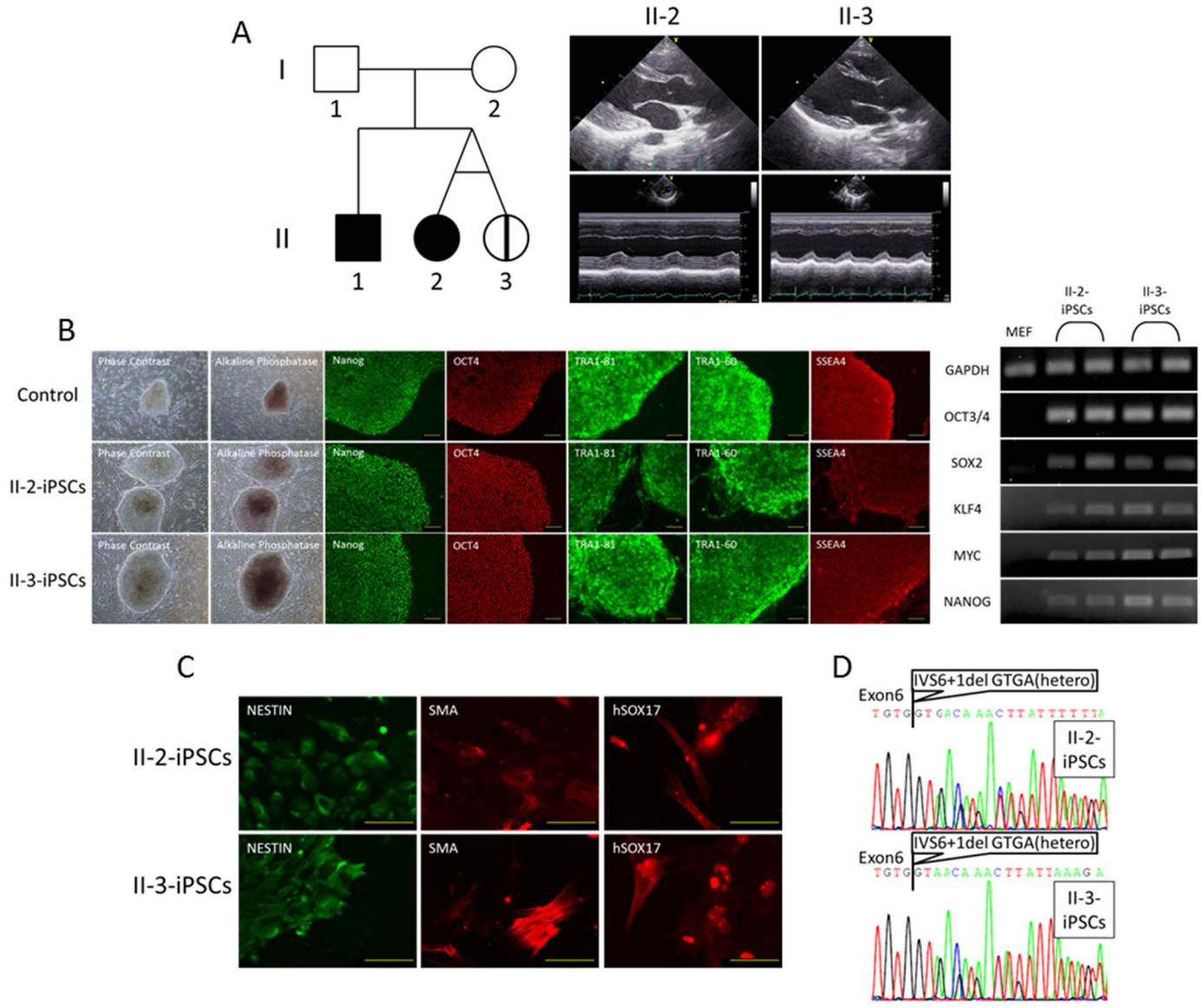

Fig. 1. Characteristics of the patients and generated iPSCs.
A, Patient pedigree and echocardiography. II-1 is the proband and II-2 and II-3 are monozygotic twins. II-2 is a symptomatic female. (Partially modified from reference 4.). II-2 showed obvious left ventricular hypertrophy, although the other did not show hypertrophy. B, Alkaline phosphatase and pluripotency marker expression were assessed by immunohistochemistry (scale = 100 μm) and RT-PCR. C, Triploblastic potential was monitored by immunofluorescence. Scale = 100 μm. D, Deletion of GTGA at the 3′ end of exon 6 was confirmed by genomic DNA sequencing of iPSCs from II-2 and II-3.

X-linked disease in vitro or not is still unknown. Additionally, previous reports demonstrate that wild-type and mutant iPSCs could be generated from single set of Rett syndrome monozygotic female twins [10,16]; however, it remains also unknown whether this is true for DD.

In the present study we generated wild-type and mutant iPSCs from clinically divergent monozygotic female twins with DD and examined the association between LAMP2 mutations and clinical presentation on the phenotype of iPSC-derived cardiomyocytes (iPSC-CMs).

2. Materials and methods

2.1. Patient characteristics

The present study examined monozygotic female twins with DD (Fig. 1A, Online Fig. 1, and Online Table 1). Echocardiography and cardiac magnetic resonance imaging (MRI) revealed cardiac hypertrophy in II-2, but not in II-3. II-2 exhibited the signs of Wolff-Parkinson-White syndrome with slightly elevated aspartate aminotransferase, lactate dehydrogenase and brain natriuretic peptide levels of 62 IU/L, 578 IU/L, and 56.1 pg/mL, respectively. II-3 showed no significant findings by echocardiography, cardiac MRI, electrocardiogram, and blood analysis [4]. This study was approved by the Research Ethics Committee of Kanazawa University (Kanazawa, Japan) and written consent obtained from each patient. All procedures were conducted in accordance with Declaration of Helsinki and the Guide for the Care and Use of Laboratory Animals published by the US National Institutes of Health (NIH Publication No. 85-23, revised 1996).

2.2. iPSC derivation and culturing

iPSCs were generated from circulating T-cells derived from each patient and control volunteer (healthy 33 year-old male) as previously reported [19]. Briefly, peripheral blood mononuclear cells (PBMCs) were isolated from whole blood samples by density gradient centrifugation with Ficoll-Paque PREMIUM Reagent (GE Healthcare, Little Chalfont, UK) according to the manufacturer's instructions. The cells

were cultured at 37 °C in 5% CO_2 with plate-bound anti-CD3 monoclonal antibody (mAb) (BD Pharmingen, NJ) in KBM502 medium (Kohjin Bio, Saitama, Japan) containing 175 JRU/mL rIL-2 to induce T-cell proliferation.

After 6 days of culture, activated PBMCs were collected and replated at 1.5×10^6 cells/well in a new 6-well plate coated with anti-CD3 mAb, incubated for an additional 24 h, and then infected with Sendai virus vectors expressing OCT3/4, SOX2, KLF4, and c-MYC (Cyte-Tune iPS Reprogramming kit; Denavec, Ibaraki, Japan). The medium was changed 24 h post-infection. At 48 h post-infection, the cells were collected and transferred to a 10 cm-dish containing mitomycin C (Sigma-Aldrich, MO)-treated mouse embryonic fibroblasts (MEFs) at 1.0×10^6 cells/dish and cultured for an additional 24 h before the medium was changed to iPSC medium containing DMEM/F12 (Sigma-Aldrich), 20% knock-out serum replacement (KSR; Invitrogen, CA), 1 mM L-glutamine (Invitrogen), 1 mM non-essential amino acids (Sigma-Aldrich), 0.1 mM β-mercaptoethanol, 50 U/mL penicillin, 50 μg/mL streptomycin (Sigma-Aldrich), and 4 ng/mL basic fibroblast growth factor (bFGF; WAKO, Osaka, Japan). The iPSCs were maintained on mitomycin C-treated MEFs in iPSC medium, which was changed every 2 days. Cells were passaged with 1 mg/mL collagenase IV (Invitrogen) every 7 days.

2.3. Immunofluoresence

Immunofluorescent staining was performed as previously reported with slight modifications [20]. Briefly, cells were fixed with 4% formaldehyde in PBS for 15 min, permeabilized with 0.1% Triton X-100 in PBS for 15 min, and blocked with 1% Bovine serum albumin in PBS for 30 min before incubating for 2 h with the following primary antibodies: Nanog (rabbit polyclonal; ReproCELL, Kanagawa, Japan), OCT3/4 (mouse monoclonal; Santa Cruz Biotechnology, Dallas, TX), TRA-1-60 (mouse monoclonal; Santa Cruz Biotechnology), TRA-1-81 (mouse monoclonal; Santa Cruz Biotechnology), SSEA-4 (mouse monoclonal; Santa Cruz Biotechnology), LAMP2 (mouse monoclonal; Abcam, Cambridge, UK), troponin T (rabbit polyclonal; Abcam), α-actinin (mouse monoclonal; Sigma-Aldrich), Nkx2.5 (rabbit polyclonal; Santa Cruz Biotechnology), H3K27me3 (rabbit polyclonal; Merck Millipore, MA) and H3K9me2 (mouse monoclonal; Abcam).

Primary antibodies were detected with Alexa Fluor 488-conjugated goat anti-rabbit IgG (H + L), Alexa Fluor 568-conjugated goat anti-mouse IgG (H + L), and Alexa Fluor 488-conjugated goat anti-mouse IgM secondary antibodies for 1 h. DAPI (Dojindo Laboratories, Kumamoto, Japan) was used for counterstaining. All procedures were performed at room temperature. Cells were also alkaline phosphatase stained by Fast Red Tablets (Roche, Basel, Switzerland). Samples were imaged using an LSM 510 META confocal microscope (ZEISS, Overkochen, Germany).

2.4. Reverse transcriptase-polymerase chain reaction (RT-PCR)

Pluripotency and cardiomyocyte (CM) gene expression were also examined by RT-PCR. Briefly, RNA was isolated using RNeasy Mini Kit (Qiagen, Venlo, Netherland) and reverse-transcribed into cDNA with QuantiTect (Qiagen). The primers used for PCR are shown in Online Table 2. LAMP2 50F-864R are primer set for exons 1–5 and LAMP2 716F-1493R are for exons 6–9. All PCR products were electrophoresed using a 2% agarose gel and visualized with ethidium bromide.

2.5. Germ layer differentiation in vitro

Germ layer differentiation was assessed in vitro by culturing iPSCs in low-attachment plates with iPSC medium to form embryoid bodies. After one week in suspension, the embryoid bodies were cultured on 0.1% gelatin-coated glass bottom dishes for one week and then fixed and stained with Nestin (rabbit polyclonal; Sigma-Aldrich), SOX17 (mouse monoclonal; R&D systems, MN), smooth muscle actin (SMA, mouse monoclonal; Dako, Glostrup, Denmark).

2.6. Genomic sequencing

Genomic DNA was isolated from iPSCs using a Gentra Puregene Cell Kit (Qiagen) and amplified with intronic primers for exons 1–9 of *LAMP2* (Online Table 3). PCR products were electrophoresed using a 2% agarose gel and purified using a QIA quick Gel Extraction kit (Qiagen) for sequencing on an ABI PRISM 310 system (Applied Biosystems, Santa Clara, CA) to confirm mutation status.

2.7. Generation of iPSC-CMs

The iPSCs were differentiated to CMs by sequential targeting of the WNT pathway as previously described with slight modifications [21]. Briefly, iPSCs were cultured in feeder-free Matrigel (BD Biosciences, NJ)-coated 6-well plates with mTeSR1 medium (STEMCELL Technologies, Vancouver, Canada) and maintained two passages to deplete MEFs. Cells were plated at 1.0×10^6/well in 6-well plates with mTeSR1 media containing 5 μM Y27632 (Cayman Chemical Company, Ann Arbor, MI). The medium was replaced daily for 5 days, and then changed to 2 mL of RPMI (Thermo Fisher Scientific, Waltham, MA) containing B27-insulin (Thermo Fisher Scientific) and 12 μM of the GSK-3 inhibitor CHIR99021 (Focus Biomolecules, Plymouth Meeting, PA)—defined as day 0. On day 1, the medium was changed to 2 mL RPMI/B27-insulin, then 1 mL of the existing medium was replaced with 1 mL fresh RPMI/B27-insulin and 5 μM of the Wnt inhibitor IWP2 (Tocris Biosciences, Bristol, UK) was added on day 3. On day5, the medium was replaced with fresh medium without IWP2 and subsequently changed every 2–3 days with RPMI/B27 + insulin (Thermo Fisher Scientific). On day 22, the medium was changed to glucose and pyruvate-free DMEM (Invitrogen) containing 4 mM lactate [22] to purify the CM-like cells. The medium was changed back to RPMI/B27 + insulin around day 26 after visual confirmation of CM-like cell purification. All cells were used in experiments at day 30–40.

2.8. iPSC-CMs size measurement

The single iPSC-CMs were re-seeded to the fibronectin (BD Biosciences) coated glassbottom dish and immunolabeled for anti-troponin T as described above. The surface areas of the single cardiomyocytes were measured by using computerized morphometric system (ImageJ software, NIH). > 50 troponin T positive iPSC-CMs were scored.

2.9. Detection of cell apoptosis

For detection of apoptosis, the iPSC-CMs were dissociated to single cells using TrypLE™ Select (Thermo Fisher Scientific) and were stained with Annexin V, Alexa Fluor™ 488 conjugate (Thermo Fisher Scientific) and the viability dye 7-AAD (Thermo Fisher Scientific). The proportion of Annexin V-positive, 7-AAD negative cells was measured by flow cytometry (Guava® easyCyte™ Flow Cytometers (Merck Millipore)). The data were analyzed using guava Soft 2.7 software. Also, TUNEL (In Situ Cell Death Detection Kit, TMR red, Sigma-Aldrich) was performed on fixed and permialized cells according to the manufacturer's instructions. This was followed by immunostaining for troponin T.

2.10. Western blotting

Cells were lysed in Pierce RIPA Buffer (Thermo Fisher Scientific) containing Halt Protease Inhibitor Cocktail (Thermo Fisher Scientific). Proteins (5 μg) were electrophoresed with 7.5% precast polyacrylamide gels (e-PAGEL, Atto-Tec, Tokyo, Japan) and transferred to PVDF (Atto-Tec). The blots were probed with anti-LAMP2 antibody and anti-alpha tubulin antibody (mouse monoclonal; Sigma-Aldrich) as a loading

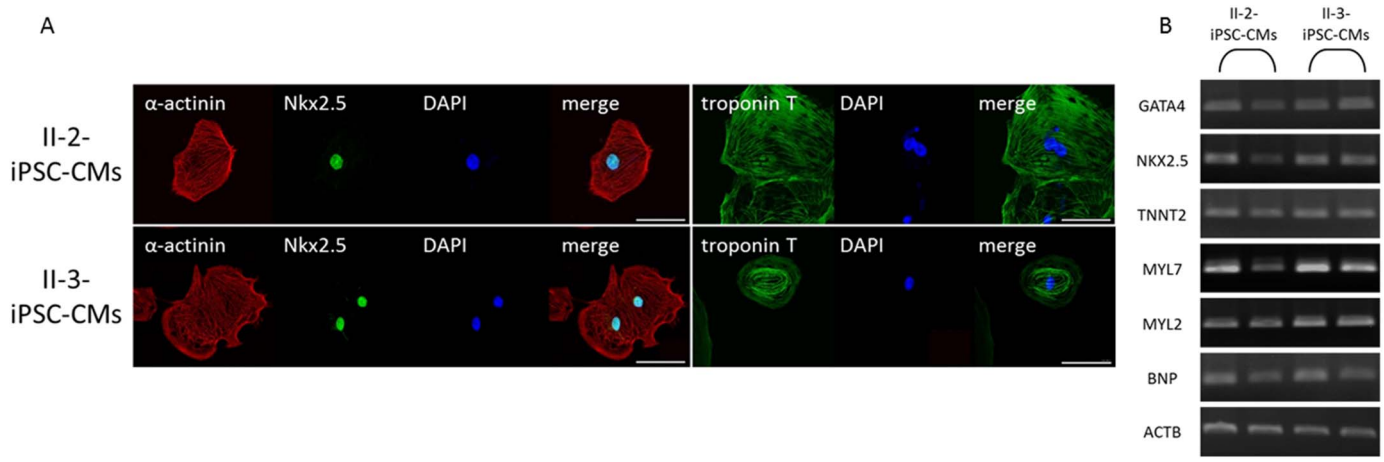

Fig. 2. Generation of iPSC-CMs.
A, Immunofluorescence (scale = 50 μm) and B, RT-PCR analysis of cardiomyocyte marker expression in both II-2 and II-3 iPSC-CMs.

standard using iBind™ Western Systems (Thermo Fisher Scientific).

2.11. In vitro autophagy analysis

Western blot and autophagic vacuole (AV) maturation were evaluated to assess autophagy dysfunction. For western blotting, whole cell lysates (20 μg) from iPSC-CMs treated with or without protease inhibitors (pepstatin A (Peptide Institute, Osaka, Japan) and E64d (Peptide Institute)) for 24 h were loaded on 4–20% gradient SDS-PAGE denaturing gels and transferred to PVDF nylon membrane using a Trans-Blot Turbo™ Blotting system (Bio-Rad, Carlsbad, CA). The membranes were blocked with 1% non-fat dry milk in PBS, and then probed with anti-LC3B (rabbit polyclonal; Medical & Biological Laboratories Co., Nagoya, Japan) primary antibody overnight at 4 °C and re-probed with anti-GAPDH antibody (Sigma-Aldrich) as a loading standard after the stripping the previous antibody. AV maturation was evaluated by tandem fluorescent-tagged LC3 (tfLC3) assay (BacMam mRFP-GFP-LC3B; Thermo Fisher Scientific). Briefly, cells were transduced for 48 h according to the manufacturer's instructions. After 2 h of starving, cells were fixed and counterstained. Early and mature AVs in 50 individual cells were evaluated by confocal microscopy and analyzed with ZEN software (ZEISS).

2.12. Transmission electron microscopy (TEM)

iPSC-CMs sections were imaged with a HITACHI H7650 (HITACHI, Tokyo, Japan) and Hitachi EMIP software (HITACHI). Only cells with visible cardiac muscle striations were assessed.

2.13. X-chromosome inactivation

X chromosome status was examined by presence of trimethyl-histone H3 (Lys27) (H3K27me3) foci in immunofluorescent staining and heterozygous (CAG)n repeats in exon 1 of the X-linked human androgen receptor (*AR*) gene. Briefly, isolated genomic DNA was treated with sodium bisulfite with a Methylamp DNA Modification Kit (Epigentek, NY). M-PCR and U-PCR primer sets (Online Table 4) were used to amplify the methylated and unmethylated *AR* alleles on the inactive and active X-chromosomes, respectively [23,24]. Amplification with the M-PCR primers will occur if the CpG dinucleotides on exon 1 of *AR* gene are methylated, and a product will be obtained only when the X chromosome is inactive, since the methylation of this region is correlated with X inactivation. Likewise, amplification with the U-PCR primers will occur if the CpG dinucleotides of *AR* gene are unmethylated, and a product will be obtained only when the X chromosome is active. The M-PCR and U-PCR forward primers were labeled at the 5′ end with a 6-carboxyfluorescein. The PCR products (1 μL) were mixed with 0.3 μL size standard (GeneScan 500LIZ dye Size Standard; Thermo Fisher Scientific), 23.5 μL Hi-Di formamide (Thermo Fisher Scientific), and 1.2 μL nuclease-free water. DNA bands were detected using an ABI PRISM 310, and peak patterns were visualized using GeneMapper software (Applied Biosystems). Skewed inactivation was based on the calculated ratio between alleles in digested DNA as follows: ≥ 75% (skewed), ≥ 80% (highly skewed), ≥ 90% extremely skewed [25].

2.14. Statistical analysis

Continuous variables are expressed as mean ± standard error of the mean (SEM). Statistical comparisons between two groups were performed using student *t*-test. $P < 0.05$ was considered statistically significant.

3. Results

3.1. Generation of iPSCs and iPSC-CMs

Typical embryonic stem cell-like iPSC colonies appeared around 20 days after gene transduction by Sendai viruses. The iPSC colonies expressed ALP and the pluripotency markers Oct3/4, Nanog, TRA1–61, TRA1–80, and SSEA-4 as determined by immunofluorescence and RT-PCR (Fig. 1B). The embryoid bodies formed from iPSCs stained positive for the triploblastic differentiate markers Nestin, SMA, and hSOX17 (Fig. 1C). A heterozygous 4-bp deletion in *LAMP2* at the intron 6 splice site (IVS6 + 1_4delGTGA) was identified in 22 iPSCs lines derived from II-2 (II-2-iPSCs) or II-3 (II-3-iPSCs) as previously reported (11 lines each; Fig. 1D) [4].

II-2-iPSCs and II-3-iPSCs started spontaneously contracting around 14 days after differentiation into cardiomyocytes (Supplementary video 1). Immunofluorescent staining revealed a marked expression in the cardiac transcription factor NKX2.5 and the sarcomeric proteins α-sarcomeric actinin and troponin T (Fig. 2A). Gene expression analysis showed an upregulation of the cardiac transcription factors, myofilaments, and hormones, including GATA4, NKX2.5, TNNT2, MYL7, MYL2 [26], and BNP (Fig. 2B) [14].

3.2. Characteristics of iPSC-CMs expressing wild-type and mutant LAMP2 from both II-2 and II-3

When iPSC-CMs were stained with LAMP2 antibody from both subjects, some lines showed aggregated signals around the nucleolus (WT-iPSCs-CMs), whereas others had no visible LAMP2 expression (MT-iPSCs-CMs) (Fig. 3A). We then selected one line each from the two

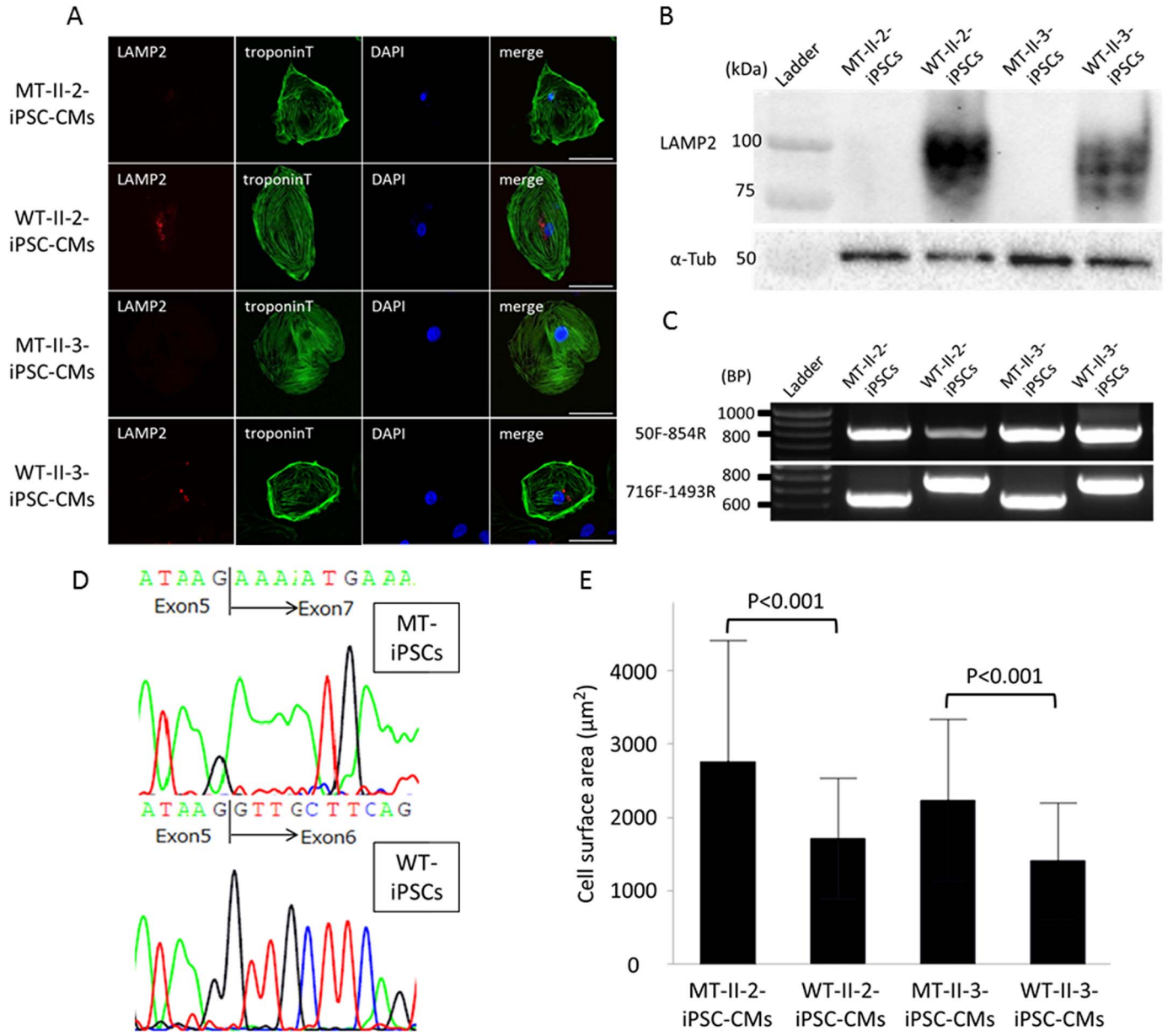

Fig. 3. Characteristics and LAMP2 mRNA and protein expression in iPSC-CMs.
A, Immunofluorescence showed some of the iPSC-CMs from each subject had aggregated LAMP-2 signals around the nucleus (WT-iPSC-CMs), however, other lines have no LAMP2 expression (MT-iPSC-CMs) (scale = 50 μm). B, Western blotting showed apparent LAMP2 protein expression in WT-iPSC-CMs but not in MT-iPSC-CMs. C, MT-iPSCs expressed amplicons around 650 bp with LAMP2 716F-1493R primers, which was smaller than expected (777 bp) on RT-PCR. D, Exon 6 skipping was proved in MT-iPSCs by cDNA sequencing. E, The cell surface area of the single MT-iPSC-CMs is significantly larger than that of WT-iPSC-CMs.

patients for western blot analysis. Notably, a ~110 kDa band consistent with LAMP2 was clearly observed in WT-iPSCs, whereas no such band was found in MT-iPSC lines (Fig. 3B). Subsequent RT-PCR analysis revealed that WT-II-2-iPSCs and WT-II-3-iPSCs expressed the expected 777 bp amplicon, while those of MT-II-2-iPSCs and MT-II-3-iPSCs were only around 650 bp (Fig. 3C) with LAMP2 716F-1493R primers. Sequence analysis confirmed that the transcriptional product from WT-iPSCs was normal, whereas exon 6 was skipped in MT-iPSCs (Fig. 3D). Interestingly, the cell surface area of single MT-iPSC-CMs is significantly larger than that of WT-iPSC-CMs (Fig. 3E). We found no significant difference in cell apoptosis between MT- and WT-iPSC-CMs in the flow cytometry assay by means of annexin V and 7-AAD and TUNEL assay (Online Fig. 2).

3.3. MT-iPSC-CMs exhibited impaired autophagy

We next examined autophagic function in the four types of iPSCs (-CMs). First, we evaluated the changes in the LC3-I and LC3-II expression in the presence of lysosome protease inhibitors (pepstatin A and E64d). No difference in LC3-II expression and LC3-II/LC3-I ratio was found between WT- and MT-iPSCs (Fig. 4A–C) with or without protease inhibitors, however, the same treatment increased LC3-II levels and LC3-II/LC3-I ratio specifically in WT-iPSC-CMs (Fig. 4D–F) and not in MT-iPSC-CMs describing abnormal autophagic maturation in MT-iPSC-CMs according to previous report [27].

Moreover, tfLC3 assay showed both immature and mature AVs in WT-iPSC-CMs; however, MT-iPSC-CMs almost exclusively contained early AVs (Fig. 4G and H). All four iPSC-CM lines exhibited sarcomere structures on TEM. Interestingly, MT-II-2-iPSC-CMs and MT-II-3-iPSC-CMs showed a significant accumulation of intracytoplasmic vacuoles,

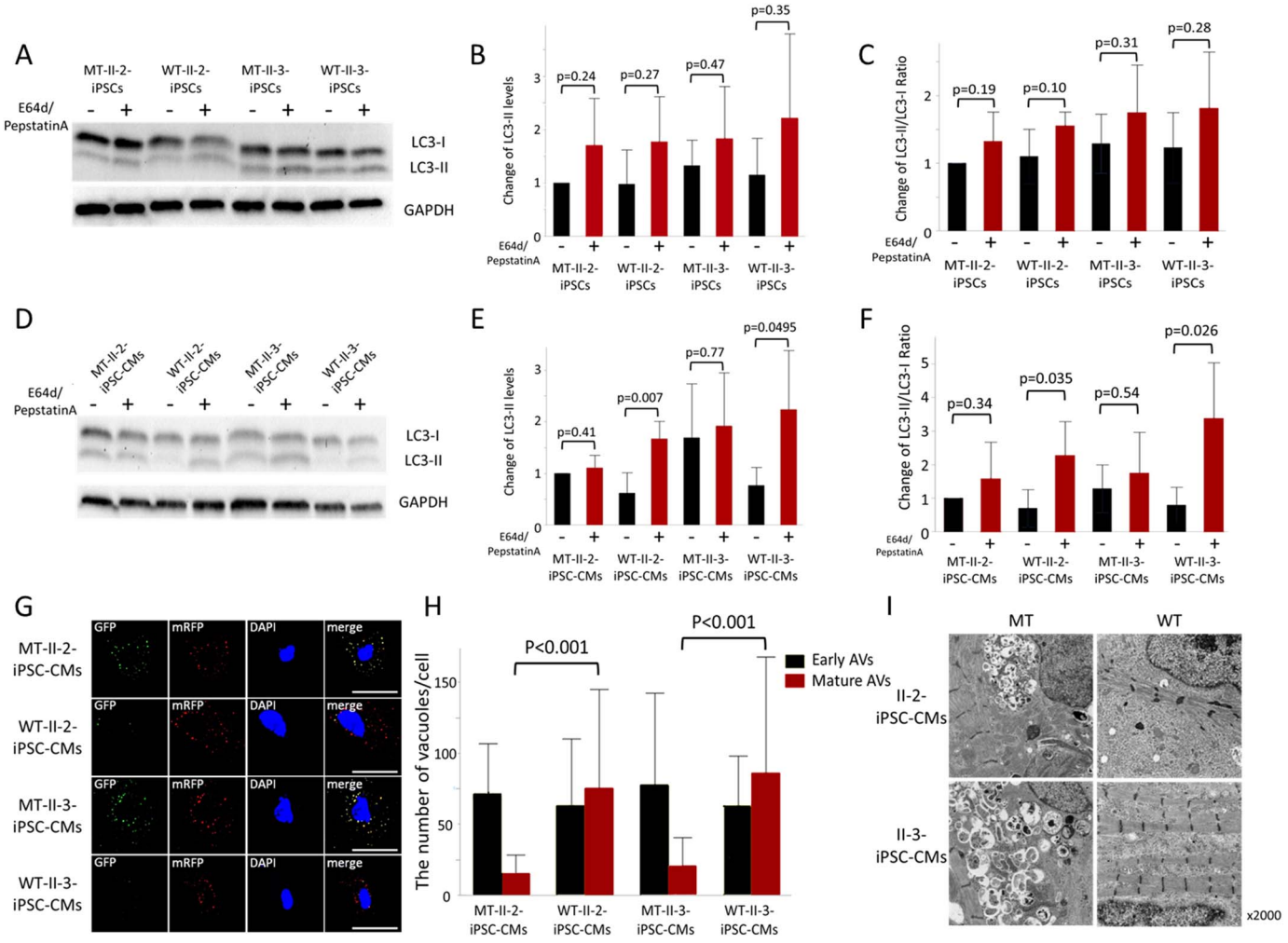

Fig. 4. Autophagic function of iPSC-CMs.
A–C, LC3 Western blotting in iPSCs. Protease inhibitor did not increase LC3-II level or LC3-II/LC3-I ratio significantly in WT-iPSCs nor MT-iPSCs. D–F, LC3 Western blotting in iPSC-CMs. LC3-II level and LC3-II/LC3-I ratio in WT-iPSC-CMs were significantly increased in the presence of protease inhibitors but not in MT-iPSC-CMs. G, H, Vacuole maturation was monitored with tfLC3 assays. WT-iPSC-CMs had both early (yellow) and mature (red) autophagic vacuoles (AVs). In contrast, MT-iPSC-CMs had significantly less number of mature AVs than that of WT-iPSC-CMs. Scale = 50 μm. I, Transmission Electron Microscopy revealed significant accumulation of intracytoplasmic vacuoles in MT-iPSC-CMs, although, there were few vacuoles in WT-iPSC-CMs. (For interpretation of the references to color in this figure legend, the reader is referred to the web version of this article.)

which were absent in WT-II-2-iPSC-CM and WT-II-3-iPSC-CM lines (Fig. 4I). As such, the vacuolation in MT-iPSC-CMs is likely to result from a failure in AV maturation owing to an absence of LAMP2 protein.

3.4. X chromosome inactivation in iPSC lines

We could confirm H3K27me3 foci by immunofluorescent staining in all II-2-iPSC and II-3-iPSC lines (Fig. 5A) describing one of the X chromosomes was inactivated. Immunostaining for dimethyl-histone H3 (Lys9) revealed homogeneous staining of the nucleus with no focus in both MT- and WT-iPSC lines (Online Fig. 3).

In the first, *AR* methylation assays were performed to PBMCs from the parents of the twins. The maternal and the paternal X chromosomes can be distinguished by polymorphism of the (CAG)n repeat element. In fact, modified DNA obtained from their father was only amplified by the U-PCR primer set with the peaks around 202 bp but not by M-PCR primer set. Likewise, modified DNA from their mother was amplified both by the U-PCR and M-PCR primer sets with the peaks around 193 and 202 bp. (Online Fig. 2). This indicated that the X chromosome with longer (CAG)n repeats in exon 1 of the *AR* gene was paternal and the X chromosome with shorter (CAG)n repeats in exon 1 of the *AR* gene was maternal. Interestingly, *AR* methylation assays revealed extremely skewed XCI patterns in all of the iPSC lines evaluated, which were not found in the isolated PBMCs. In addition, MT-iPSCs displayed a methylated (inactivated) X chromosome of paternal origin, whereas WT-iPSCs harbored a methylated (inactivated) X chromosome of maternal origin, regardless of the twin from which they derived (Table 1 and Fig. 5B).

4. Discussion

In the present study, we successfully generated iPSCs from monozygotic twins with DD (II-2 and II-3) that showed divergent clinical phenotypes especially regarding cardiac phenotypes. Under these conditions, the generated iPSCs could be categorized into 4 groups—MT-II-2-iPSCs, WT-II-2-iPSCs, MT-II-3-iPSCs, and WT-II-3-iPSCs—where MT-iPSCs and WT-iPSCs from both twins expressed mutant or wild-type LAMP2, respectively. Autophagy failure was observed only in MT-iPSC-CMs by tandem fluorescent-tagged LC3 analysis and LC3-II western blotting. Moreover, the intracytoplasmic vacuoles which are common findings in the histological sections of the heart of the patients with DD were also observed in MT-iPSC-CMs from each twin. Under these conditions, the existence of H3K27me3 foci revealed that one of the X chromosomes was inactivated and that there was no impairment of dosage compensation, which is a mechanism to equalize the expression of X-chromosome in males and females. In combination with the

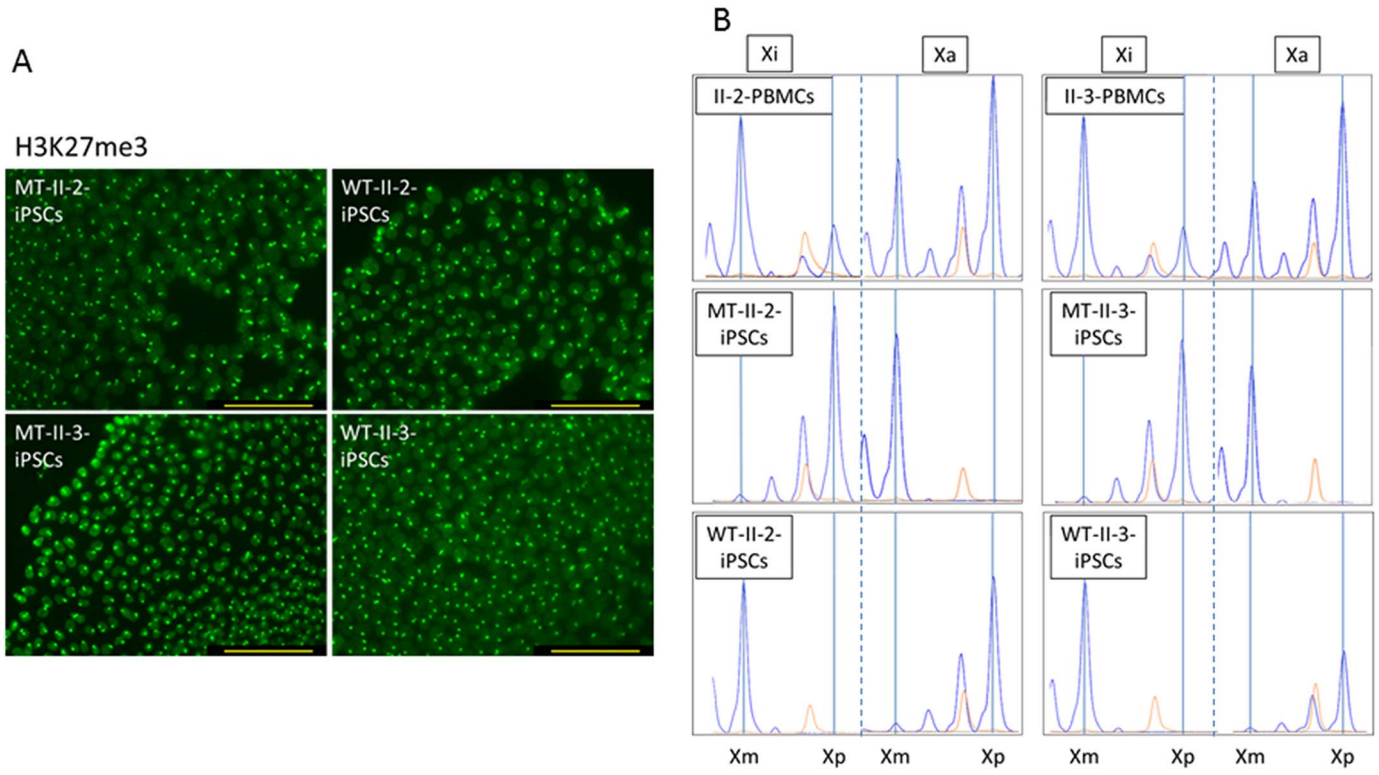

Fig. 5. X-chromosome inactivation (XCI) status of generated iPSCs.
A, H3K27me3 immunostaining in iPSCs. H3K27me3 foci were detected in all the lines of generated iPSCs. (II-2 and II-3 iPSCs). B, *AR* methylation assay. The XCI patterns of peripheral blood mononuclear cells (PBMCs) were not skewed. Different from them, the XCI patterns of MT-iPSCs were extremely skewed that X chromosome of paternal origin (Xp) was inactivated and X chromosome of maternal origin (Xm) was activated. Opposed to MT-iPSCs, Xm was extremely inactivated and Xp was extremely activated on WT-iPSCs regardless of their host. Size standard (yellow peak) = 200 bp. (For interpretation of the references to color in this figure legend, the reader is referred to the web version of this article.)

Table 1
X-chromosome inactivation (XCI) patterns of peripheral blood mononuclear cells (PBMCs) and induced pluripotent stem cells (iPSCs) assessed by *AR* methylation assay.

Cell lines	XCI pattern ratio	Assessment	Active X chromosome origin
II-2-PBMCs	29:71	Not skewed	–
II-3-PBMCs	29:71	Not skewed	–
MT-II-2-iPSCs	99:1	Extremely skewed	Mother
WT-II-2-iPSCs	0:100	Extremely skewed	Father
MT-II-3-iPSCs	98:2	Extremely skewed	Mother
WT-II-3-iPSCs	0:100	Extremely skewed	Father

H3K27me3 immunostaining, *AR* methylation assay revealed that the normal paternal X chromosome was inactivated in MT-iPSC-CMs. This inactivation could elucidate the result that only MT-iPSC-CMs from both twins demonstrated in vitro phenotypes of DD.

The autophagy impairment was detected in the MT-iPSC-CMs. Moreover, MT-iPSC-CMs had larger cell surface area than that of WT-iPSC-CMs. According to the previous study, altered autophagy was indicated not only in the autophagy related gene defecting disease like DD but also in the sarcomeropathy related hypertrophic cardiomyopathy [28]. Also, several cardiac storage disorders demonstrate cardiac hypertrophy [29,30]. Especially, the autophagic vacuoles of DD are strongly related to the alteration of autophagy [2]. Therefore, the cardiomyocyte hypertrophy subsequent to the autophagy impairment of MT-iPSC-CMs contributed to the hypertrophic cardiomyopathy of patient II-2. Direct sample of the cardiomyocyte of the twins to evaluate the XCI patterns and the morphologic differences is necessary to approve our hypotheses.

There was no significant difference in cell apoptosis between MT- and WT-iPSC-CMs in the present study, although the previous study had shown that Danon iPSC-CMs displayed markedly higher TUNEL staining than WT control lines [14]. One of the reasons for the difference can be explained by the differences in the site of gene mutation. The additional stress that induces further apoptosis may cause apoptotic difference between MT- and WT-iPSC-CMs in our experimental system [31].

The human LAMP2 gene is located on chromosome Xq24 and its pre-mRNA is alternatively spliced into three isoforms. Translated LAMP2 variants are single-pass lysosomal membrane proteins involved in autophagic flux by contributing the autophagosome/lysosomal membrane interactions and autophagosome clearance. Interestingly, impairment in autophagosome maturation was shown in MT-iPSC-CMs but not in MT-iPSCs, although the LAMP2 mutation was already demonstrated on MT-iPSCs. Possible reasons for the phenomenon are as follows. First, CMs exhibit abundant LAMP2 protein expression—particularly the LAMP-2B isoform [32]. Second, in CMs, autophagy occurs at basal levels and the basal autophagy play a critical role in cardiomyocyte function and survival [33,34]. Last, it is well known that mitochondria are abundant in CMs. The most recent study showed the mitochondrial damage/dysfunction and incomplete mitophagy contribute to the disruption of macroautophagy in iPSC-CMs derived from patient with DD [35]. From these observations, the observed differences in LAMP2 expression, autophagic activity, and the amount of mitchondria might affect the impaired autophagy in both MT-iPSC-CMs but not in MT-iPSCs from each twin with DD.

In the present study, II-2 and II-3 were identical twins and they both have mutated LAMP2, however, only II-2 showed hypertrophic cardiomyopathy. The difference in the clinical phenotype might also explain from single nucleotide polymorphism of the twins. Nevertheless,

considering the result that we could generate similar MT- and WT-iPSCs from each twin, the epigenetic difference represented by X chromosome inactivation probably contributes to the distinct clinical phenotype. Furthermore, the clinical divergency of the twins did not correlate to the in vitro iPSC-CMs phenotype, which led us to two hypotheses. First, different organs in an individual have distinct XCI patterns [36]. In other words, it is difficult to estimate the XCI patterns of certain organ from clinical phenotype in other organs caused by X-linked disease. Indeed, II-2 and II-3 had similar non-skewed XCI patterns in peripheral blood leukocytes and both LAMP2-negative and LAMP2-positive granulocytes were observed by flow cytometry in spite of their different clinical cardiomyopathy phenotypes [4].

Second, regardless of XCI patterns of the host somatic cells, the state of X chromosome changes dynamically during generation of human female iPSCs. Successful reprogramming of differentiated somatic cells is thought to require epigenetic remodeling, including reactivation of the inactive X [37]. According to the previous reports [15,38,39], random re-inactivation of one X chromosomes occurs subsequent to X chromosome reactivation on human iPSCs, suggesting that the XCI states are reset by reprograming, explaining why these MT- and WT-iPSCs (− CMs) had different XCI. Thus, our data demonstrate that with or without clinical phenotype, the X chromosome that either paternal or maternal originated allele was inactivated may reactivate during reprograming, and then one X chromosome could be randomly inactivated during several passages.

Theoretically, most colonies should be heterogeneous with both maternal and paternal X chromosome inactivation, assuming XCI occurs at random. However, in conjunction with a previous report [38], XCI states of both iPSCs from DD twins were extremely skewed to maternal or paternal X chromosome. Therefore, we suggest that each iPSC colony was derived from a single somatic cell, although it remains unclear how X chromosomes are selected for inactivation. Under these conditions, appropriate inactivation of pathogenic X chromosome and reactivation of normal X chromosome probably contribute to the treatment of female X-linked diseases such as present cases. In fact, 5-aza-2′-deoxycytidine induced *LAMP2* demethylation and restored expression in both iPSCs and iPSC-CMs derived from female DD fibroblasts in vitro [40]. However, the effect of the demethylating agents is global and potential off-target effects may present some clinical concerns. Therefore, agents that could specifically target the non-desirable X chromosome for inactivation would be key in treating X-linked diseases.

5. Conclusion

We successfully established two sets of iPSC lines that expressed either wild-type or mutant LAMP2 allele from each monozygotic female twin with DD, of which only the populations expressing mutant LAMP2 showed autophagic failure. The XCI patterns of the iPSCs elucidate the LAMP2 expression and subsequent in vitro phenotype. The in vitro characteristics of generated iPSCs and iPSC-CMs did not rely on the clinical phenotype of each twin. The fact that we could generate disease specific iPSCs with evident in vitro phenotype from patient with X-linked disease without clinical phenotype is a great advantage of this experimental system to investigate the disease mechanism. Although, these findings aroused attention developing disease-specific iPSCs derived from female with not only X-linked disease represented by DD but also autosomal chromosome related disease, that is, harbored mutation on X chromosome could be remarkable after generating iPSCs. Careful evaluation of the in vitro phenotype is mandatory when using iPSCs derived from female human as a model of the disease.

Supplementary data to this article can be found online at https://doi.org/10.1016/j.yjmcc.2017.11.019.

Sources of funding

This work was supported by a MEXT KAKENHI Grant-in-Aid for Young Scientists (No. JP16K19632).

Disclosures

None to disclose.

Acknowledgments

We thank Dr. Shinsuke Yuasa (Department of Cardiology, Keio University School of Medicine) for valuable technical support.

References

[1] M.J. Danon, Oh. SJ, S. DiMauro, J.R. Manaligod, A. Eastwood, S. Naidu, et al., Lysosomal glycogen storage disease with normal acid maltase, Neurology 31 (1981) 51–57.
[2] I. Nishino, J. Fu, K. Tanji, T. Yamada, S. Shimojo, T. Koori, et al., Primary LAMP-2 deficiency causes X-linked vacuolar cardiomyopathy and myopathy (Danon disease), Nature 406 (2000) 906–910.
[3] R.S. D'Souza, C. Levandowski, D. Slavov, S.L. Graw, L.A. Allen, E. Adler, et al., Danon disease: clinical features, evaluation, and management, Circ. Heart Fail. 7 (2014) 843–849.
[4] Y. Hashida, T. Wada, T. Saito, K. Ohta, Y. Kasahara, A. Yachie, Early diagnosis of Danon disease: flow cytometric detection of lysosome-associated membrane protein-2-negative leukocytes, J. Cardiol. 66 (2015) 168–174.
[5] K. Takahashi, S. Yamanaka, Induction of pluripotent stem cells from mouse embryonic and adult fibroblast cultures by defined factors, Cell 126 (2006) 663–676.
[6] J. Yu, M.A. Vodyanik, K. Smuga-Otto, J. Antosiewicz-Bourget, J.L. Frane, S. Tian, et al., Induced pluripotent stem cell lines derived from human somatic cells, Science 318 (2007) 1917–1920.
[7] N. Tsumaki, M. Okada, A. Yamashita, iPS cell technologies and cartilage regeneration, Bone 70 (2015) 48–54.
[8] B.S. Freedman, Modeling kidney disease with iPS cells, Biomark. Insights 10 (2015) 153–169.
[9] S. Arai, M. Miyauchi, M. Kurokawa, Modeling of hematologic malignancies by iPS technology, Exp. Hematol. 43 (2015) 654–660.
[10] T. Andoh-Noda, W. Akamatsu, K. Miyake, T. Matsumoto, R. Yamaguchi, T. Sanosaka, et al., Differentiation of multipotent neural stem cells derived from Rett syndrome patients is biased toward the astrocytic lineage, Mol. Brain 8 (2015) 31.
[11] K. Sallam, K. Kodo, J.C. Wu, Modeling inherited cardiac disorders, Circ. J. 78 (2014) 784–794.
[12] C.S. Young, M.R. Hicks, N.V. Ermolova, H. Nakano, M. Jan, S. Younesi, et al., A single CRISPR-Cas9 deletion strategy that targets the majority of DMD patients restores dystrophin function in hiPSC-derived muscle cells, Cell Stem Cell 18 (2016) 533–540.
[13] B. Jia, S. Chen, Z. Zhao, P. Liu, J. Cai, D. Qin, et al., Modeling of hemophilia a using patient-specific induced pluripotent stem cells derived from urine cells, Life Sci. 108 (2014) 22–29.
[14] S.I. Hashem, C.N. Perry, M. Bauer, S. Han, S.D. Clegg, K. Ouyang, et al., Brief report: oxidative stress mediates cardiomyocyte apoptosis in a human model of Danon disease and heart failure, Stem Cells 33 (2015) 2343–2350.
[15] S. Mekhoubad, C. Bock, A.S. de Boer, E. Kiskinis, A. Meissner, K. Eggan, Erosion of dosage compensation impacts human iPSC disease modeling, Cell Stem Cell 10 (2012) 595–609.
[16] G. Ananiev, E.C. Williams, H. Li, Q. Chang, Isogenic pairs of wild type and mutant induced pluripotent stem cell (iPSC) lines from Rett syndrome patients as in vitro disease model, PLoS One 6 (2011) e25255.
[17] M. Reboun, J. Rybova, R. Dobrovolny, J. Vcelak, T. Veselkova, G. Storkanova, et al., X-chromosome inactivation analysis in different cell types and induced pluripotent stem cells elucidates the disease mechanism in a rare case of Mucopolysaccharidosis type II in a female, Folia Biol. 62 (2016) 82–89.
[18] I.H. Park, N. Arora, H. Huo, N. Maherali, T. Ahfeldt, A. Shimamura, et al., Disease-specific induced pluripotent stem cells, Cell 134 (2008) 877–886.
[19] T. Seki, S. Yuasa, M. Oda, T. Egashira, K. Yae, D. Kusumoto, et al., Generation of induced pluripotent stem cells from human terminally differentiated circulating T cells, Cell Stem Cell 7 (2010) 11–14.
[20] N. Sun, N.J. Panetta, D.M. Gupta, K.D. Wilson, A. Lee, F. Jia, et al., Feeder-free derivation of induced pluripotent stem cells from adult human adipose stem cells, Proc. Natl. Acad. Sci. U. S. A. 106 (2009) 15720–15725.
[21] X. Lian, J. Zhang, S.M. Azarin, K. Zhu, L.B. Hazeltine, X. Bao, et al., Directed cardiomyocyte differentiation from human pluripotent stem cells by modulating Wnt/beta-catenin signaling under fully defined conditions, Nat. Protoc. 8 (2013) 162–175.
[22] S. Tohyama, F. Hattori, M. Sano, T. Hishiki, Y. Nagahata, T. Matsuura, et al., Distinct metabolic flow enables large-scale purification of mouse and human pluripotent stem cell-derived cardiomyocytes, Cell Stem Cell 12 (2013) 127–137.
[23] K. Sato, M. Hashiyada, S. Uehara, M. Nata, K. Okamura, CpG dinucleotide

methylation patterns in the human androgen receptor gene and X-chromosome inactivation in peripheral blood leukocytes of phenotypically normal women, J. Hum. Genet. 48 (2003) 374–379.
[24] T. Kubota, S. Nonoyama, H. Tonoki, M. Masuno, K. Imaizumi, M. Kojima, et al., A new assay for the analysis of X-chromosome inactivation based on methylation-specific PCR, Hum. Genet. 104 (1999) 49–55.
[25] L.A. Kiedrowski, G. Raca, J.J. Laffin, B.S. Nisler, K. Leonhard, E. McIntire, et al., DNA methylation assay for X-chromosome inactivation in female human iPS cells, Stem Cell Rev. 7 (2011) 969–975.
[26] J. Zhang, M. Klos, G.F. Wilson, A.M. Herman, X. Lian, K.K. Raval, et al., Extracellular matrix promotes highly efficient cardiac differentiation of human pluripotent stem cells: the matrix sandwich method, Circ. Res. 111 (2012) 1125–1136.
[27] S. Kimura, N. Fujita, T. Noda, T. Yoshimori, Monitoring autophagy in mammalian cultured cells through the dynamics of LC3, Methods Enzymol. 452 (2009) 1–12.
[28] S.R. Singh, A.T.L. Zech, B. Geertz, S. Reischmann-Dusener, H. Osinska, M. Prondzynski, et al., Activation of autophagy ameliorates cardiomyopathy in Mybpc3-targeted Knockin mice, Circ. Heart Fail. 10 (2017) e004100.
[29] S.J. Chou, W.C. Yu, Y.L. Chang, W.Y. Chen, W.C. Chang, Y. Chien, et al., Energy utilization of induced pluripotent stem cell-derived cardiomyocyte in Fabry disease, Int. J. Cardiol. 232 (2017) 255–263.
[30] B.J. Byrne, P.S. Kishnani, L.E. Case, L. Merlini, W. Muller-Felber, S. Prasad, et al., Pompe disease: design, methodology, and early findings from the Pompe registry, Mol. Genet. Metab. 103 (2011) 1–11.
[31] C.Y. Law, C.W. Siu, K. Fan, W.H. Lai, K.W. Au, Y.M. Lau, et al., Lysosomal membrane permeabilization is involved in oxidative stress-induced apoptotic cell death in LAMP2-deficient iPSCs-derived cerebral cortical neurons, Biochem. Biophys. Rep. 5 (2016) 335–345.
[32] D.S. Konecki, K. Foetisch, K.P. Zimmer, M. Schlotter, U. Lichter-Konecki, An alternatively spliced form of the human lysosome-associated membrane protein-2 gene is expressed in a tissue-specific manner, Biochem. Biophys. Res. Commun. 215 (1995) 757–767.
[33] A. Nakai, O. Yamaguchi, T. Takeda, Y. Higuchi, S. Hikoso, M. Taniike, et al., The role of autophagy in cardiomyocytes in the basal state and in response to hemodynamic stress, Nat. Med. 13 (2007) 619–624.
[34] S. Lavandero, R. Troncoso, B.A. Rothermel, W. Martinet, J. Sadoshima, J.A. Hill, Cardiovascular autophagy: concepts, controversies, and perspectives, Autophagy 9 (2013) 1455–1466.
[35] S.I. Hashem, A.N. Murphy, A.S. Divakaruni, M.L. Klos, B.C. Nelson, E.C. Gault, et al., Impaired mitophagy facilitates mitochondrial damage in Danon disease, J. Mol. Cell. Cardiol. 108 (2017) 86–94.
[36] M. Satoh, S. Ogikubo, A. Yoshizawa-Ogasawara, Correlation between clinical phenotypes and X-inactivation patterns in six female carriers with heterozygote vasopressin type 2 receptor gene mutations, Endocr. J. 55 (2008) 277–284.
[37] N. Maherali, R. Sridharan, W. Xie, J. Utikal, S. Eminli, K. Arnold, et al., Directly reprogrammed fibroblasts show global epigenetic remodeling and widespread tissue contribution, Cell Stem Cell 1 (2007) 55–70.
[38] K.Y. Kim, E. Hysolli, Y. Tanaka, B. Wang, Y.W. Jung, X. Pan, et al., X chromosome of female cells shows dynamic changes in status during human somatic cell reprogramming, Stem Cell Rep. 2 (2014) 896–909.
[39] C. Vallot, J.F. Ouimette, M. Makhlouf, O. Feraud, J. Pontis, J. Come, et al., Erosion of X chromosome inactivation in human pluripotent cells initiates with XACT coating and depends on a specific heterochromatin landscape, Cell Stem Cell 16 (2015) 533–546.
[40] K.M. Ng, P.Y. Mok, A.W. Butler, J.C. Ho, S.W. Choi, Y.K. Lee, et al., Amelioration of X-linked related autophagy failure in Danon disease with DNA methylation inhibitor, Circulation 134 (2016) 1373–1389.